Supplement of Atmos. Chem. Phys., 25, 4755–4766, 2025
https://doi.org/10.5194/acp-25-4755-2025-supplement

Atmospheric Chemistry and Physics
Open Access

Supplement of

Measurement report: Size-resolved particle effective density measured by an AAC-SMPS and implications for chemical composition

Yao Song et al.

Correspondence to: Lingling Jin (jinlingling@zjemc.org.cn) and Zhibin Wang (wangzhibin@zju.edu.cn)

1 Derivation of effective density from d_m and d_{ae}

The AAC is a novel instrument that selects the aerodynamic equivalent diameter of aerosol particles on the basis of their relaxation time (Tavakoli and Olfert, 2013). The AAC consists of two cylinders rotating in the same direction at the same speed, and it classifies particles on the basis of relaxation time, which is defined by

$$\tau = Bm = \frac{\mathrm{Cc}(d_{\mathrm{ae}})\rho_0 d_{\mathrm{ae}}^2}{18\mu}, \quad \text{(S1)}$$

where μ is the viscosity of air. Cc(d_{ae}) is the slip correction factor. where ρ_0 is the standard density with a value of 1 g/cm^3 (Johnson et al. 2018). B is the mobility, which can be expressed as

$$\mathrm{B} = \frac{Cc(d_m)}{3\pi\mu d_m}, \quad \text{(S2)}$$

where d_{m} is the mobility diameter. Then, ρ_{eff} can be derived by combining equations 2 and 3:

$$\rho_{\mathrm{eff}} = \frac{m}{\frac{\pi}{6}d_m^3} = \frac{Cc(d_{\mathrm{ae}})\rho_0 d_{\mathrm{ae}}^2}{Cc(d_{\mathrm{m}})d_{\mathrm{m}}^2}, \quad \text{(S3)}$$

where d_{m} denotes the mode value of the number–mobility size distribution for d_{ae}-selected particles, which was determined using AAC-SMPS. The number–mobility size distributions were measured and fitted to log-normal distributions. The equation of the log-normal distribution used in this study is expressed as

$$N(D_{\mathrm{m}}) = \frac{N_0}{\sqrt{2\pi}\ln\sigma}\exp\left(\frac{-(\log(D_{\mathrm{m}})-\log(d_{\mathrm{m}}))^2}{2(\ln\sigma)^2}\right), \quad \text{(S4)}$$

where D_{m} is each setpoint of mobility size scanned by the SMPS. σ is the geometric standard deviation of the D_{m} distributions. d_{m} represents the geometric mean of D_{m}.

The aerodynamic diameter can be calculated from the particle relaxation time according to Eq. S2. Applying the propagation of uncertainty, the uncertainty of d_{ae} can be derived as follows,

$$\left(\frac{\varepsilon_{d_{\mathrm{ae}}}}{d_{\mathrm{ae}}}\right)^2 = \frac{1}{4}\left(\frac{\varepsilon_\tau}{\tau}\right)^2 + \frac{1}{4}\left(\frac{\varepsilon_\mu}{\mu}\right)^2 + \frac{1}{4}\left(\frac{\varepsilon_{Cc}}{Cc}\right)^2, \quad \text{(S5)}$$

where $\varepsilon\mu/\mu$ = 1.2%, εCc/Cc is the same for all particle sizes and equals 2.1%, and $\varepsilon\tau/\tau$ is associated with the sheath flow rate Q_{sh}, rotating rate ω and dimensional parameters (length L and mean radius of inner and outer cylinders $\bar{r}$) of AAC

$$\left(\frac{\varepsilon_\tau}{\tau}\right)^2 = \left(\frac{\varepsilon_{Q_{sh}}}{Q_{sh}}\right)^2 + 4\left(\frac{\varepsilon_\omega}{\omega}\right)^2 + 4\left(\frac{\varepsilon_{\bar{r}}}{\bar{r}}\right)^2 + \left(\frac{\varepsilon_L}{L}\right)^2, \quad \text{(S6)}$$

where $\varepsilon Q_{\mathrm{sh}}$ = 0.1 Lpm, $\varepsilon\omega$ = 5 rpm, εL = 2 mm, and $\varepsilon_{\bar{r}}$ = 5 μm.

According to Eq. S1, the uncertainty for particle mass is

$$\left(\frac{\varepsilon_m}{m}\right)^2 = \left(\frac{\varepsilon_\tau}{\tau}\right)^2 + \left(\frac{\varepsilon_B}{B}\right)^2, \quad \text{(S7)}$$

and $\frac{\varepsilon_B}{B}$ can be written as follows according to Eq. S2,

$$\left(\frac{\varepsilon_B}{B}\right)^2 = \left(\frac{\varepsilon_{Cc}}{Cc}\right)^2 + \left(\frac{\varepsilon_\mu}{\mu}\right)^2 + \left(\frac{\varepsilon_{d_m}}{d_m}\right)^2, \quad \text{(S8)}$$

where $\frac{\varepsilon_{d_m}}{d_m}$ = 3%.

As a result, the uncertainty in effective density is

$$(\frac{\varepsilon_{\rho_{\mathrm{eff}}}}{\rho_{\mathrm{eff}}})^2 = 9(\frac{\varepsilon d_m}{d_m})^2 + (\frac{\varepsilon_m}{m})^2. \quad \text{(S9)}$$

As the sheath flow rate used in this study is a constant, there is not much difference among the uncertainty for effective densities of selected particles with different sizes (Table S1).

Table S1: the uncertainty for effective densities of selected particles with different sizes measured by the AAC-SMPS.

d_{ae} (nm)	τ (%)	ρ (%)
200	1.50	3.00
235	1.51	3.00
277	1.52	3.01
326	1.52	3.01
384	1.54	3.02
452	1.57	3.03
531	1.59	3.05

2. Source apportionment of organic aerosols

The OA data were processed using Tofware_v3_3_0_ACSM. Positive matrix factorization (PMF) analysis was performed using an Igor Pro-based PMF evaluation toolkit (PET v3.04) on high-resolution mass spectra of OA with m/z ranging from 12 to 100. The method described in detail can be found in Zhang et al. (2024). A total of 6 sources were identified, including hydrocarbon-like OA (HOA), cooking OA (COA), nitrogen-containing OA (NOA), oxidized primary organic aerosol (OPOA), more oxidized oxygenated organic aerosol (MO-OOA) and less oxidized oxygenated organic aerosol (LO-OOA).

Table S2: The best hyperparameters of the RF model and R^2 values for particles of different sizes.

d_{ae} (nm)	n_estimators	min_samples_leaf	max_samples	max_features	max_depth	R^2
200	100	2	0.75	sqrt	9	0.78
235	100	2	0.75	sqrt	7	0.71
277	400	2	0.75	sqrt	8	0.65
326	300	2	0.75	sqrt	8	0.55
384	300	2	0.75	sqrt	10	0.42
452	400	2	0.75	sqrt	7	0.32
531	400	2	0.75	sqrt	9	0.22

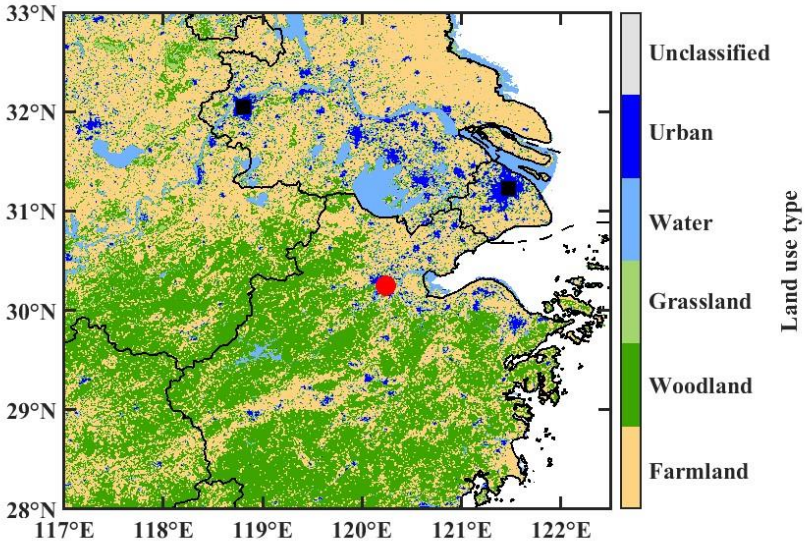

Figure S1: Geographical location of the measurement site.

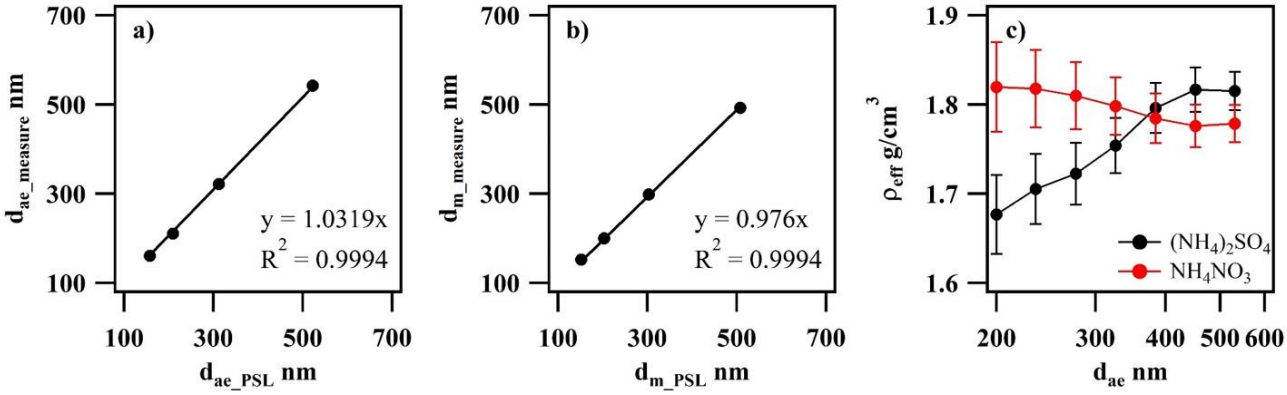

Figure S2: Calibration of the (a) AAC and (b) SMPS using PSL particles. (c) Size-resolved ρ_{eff} values of the $(NH_4)_2SO_4$ and NH_4NO_3 particles measured by AAC-SMPS.

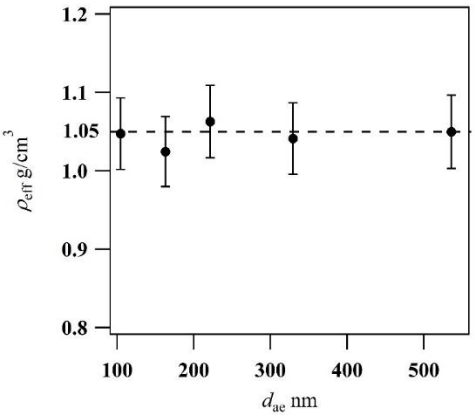

Figure S3: Size-resolved ρ_{eff} values of PSL particles measured by AAC-SMPS

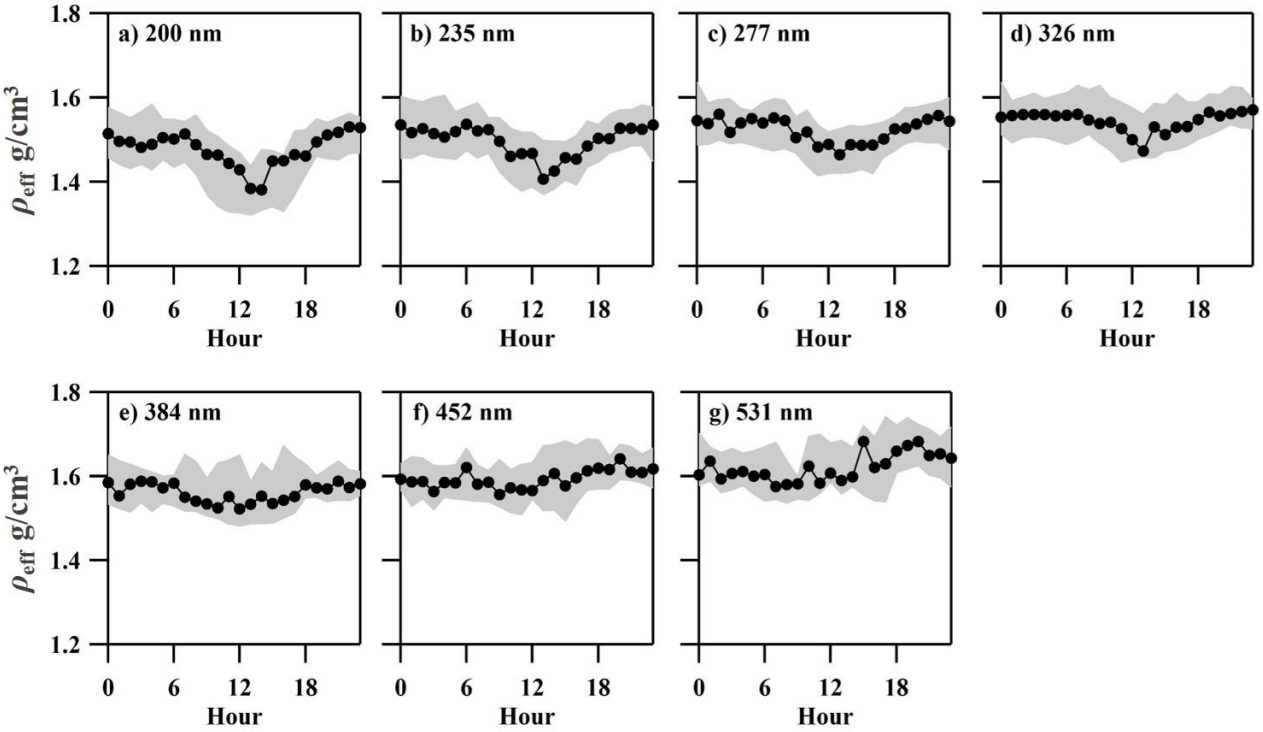

Figure S4 Diurnal variations in the size-resolved effective density of particles with diameters of (a) 200 nm, (b) 235 nm, (c) 277 nm, (d) 326 nm, (e) 384 nm, (f) 452 nm, and (g) 531 nm.

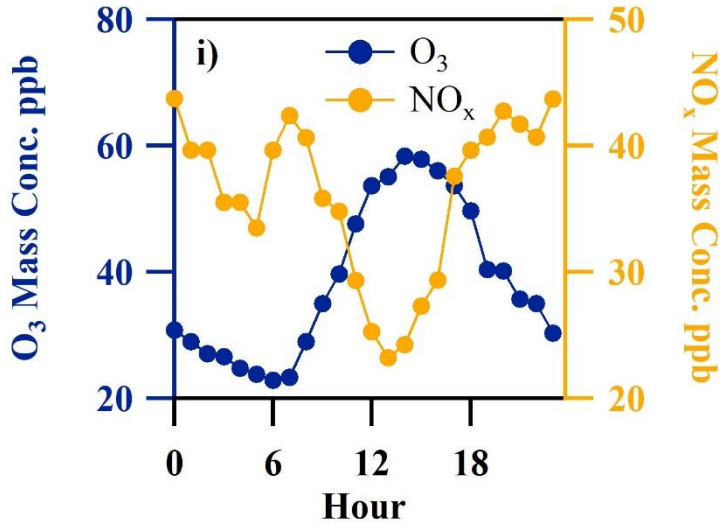

Figure S5: Diurnal variations in O_3 and NOx concentrations.

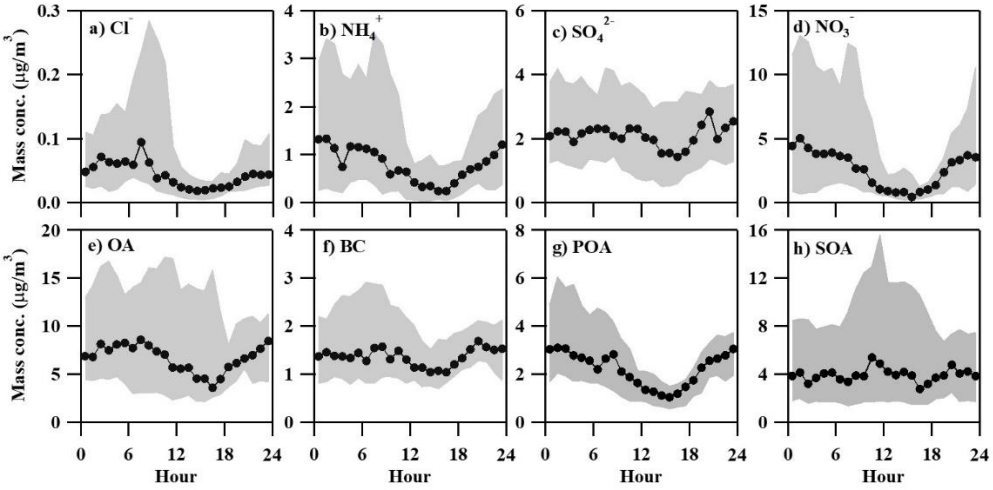

Figure S6: Diurnal variations in the mass concentrations of (a) Cl^-, (b) NH_4^+, (c) SO_4^{2-}, (d) NO_3^-, (e) OA measured by ACSM, (f) BC measured by AE-33, (g) POA and (h) SOA resolved from PMF analysis on organic mass spectra.

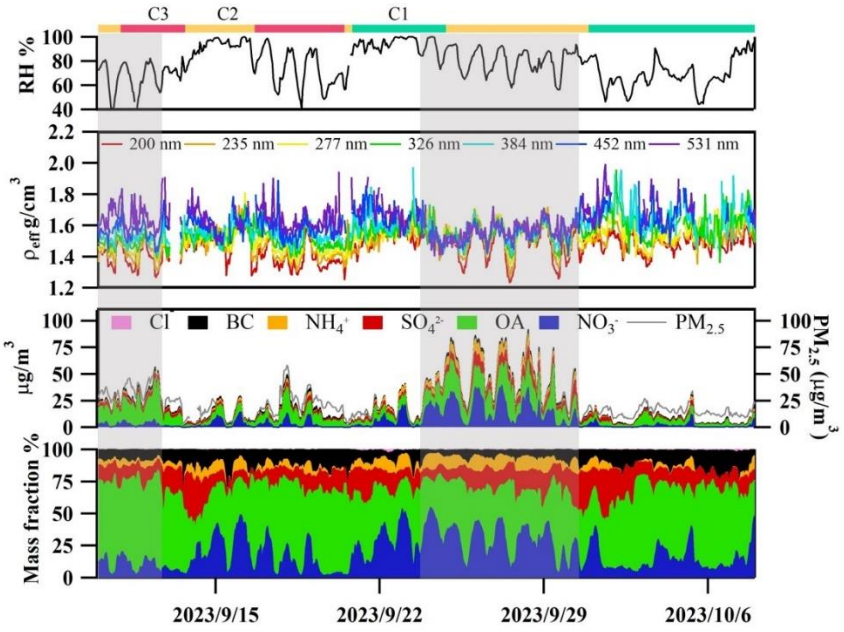

Figure S7: Time series of (a) humidity, (b) size-resolved ρ_{eff} of particles, (c) mass concentrations of $PM_{2.5}$ and different chemical compositions, and (d) mass fractions of different species.

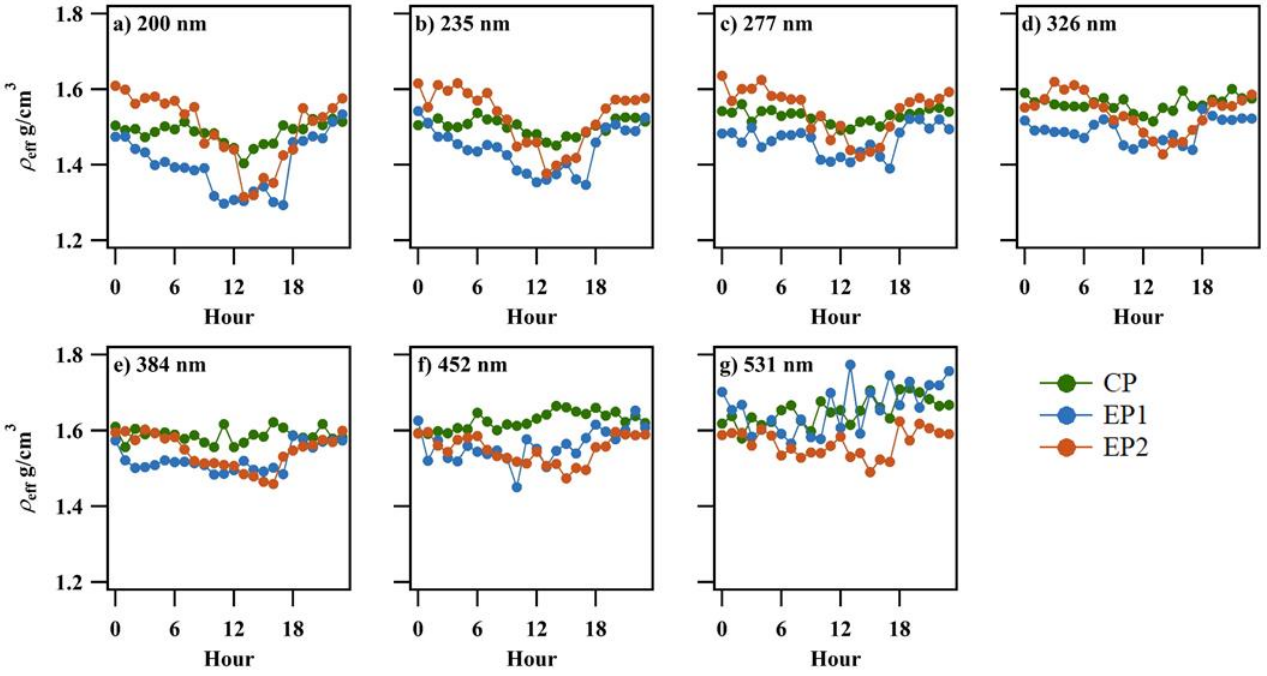

Figure S8: Diurnal variations in the effective densities of particles at different pollution levels.

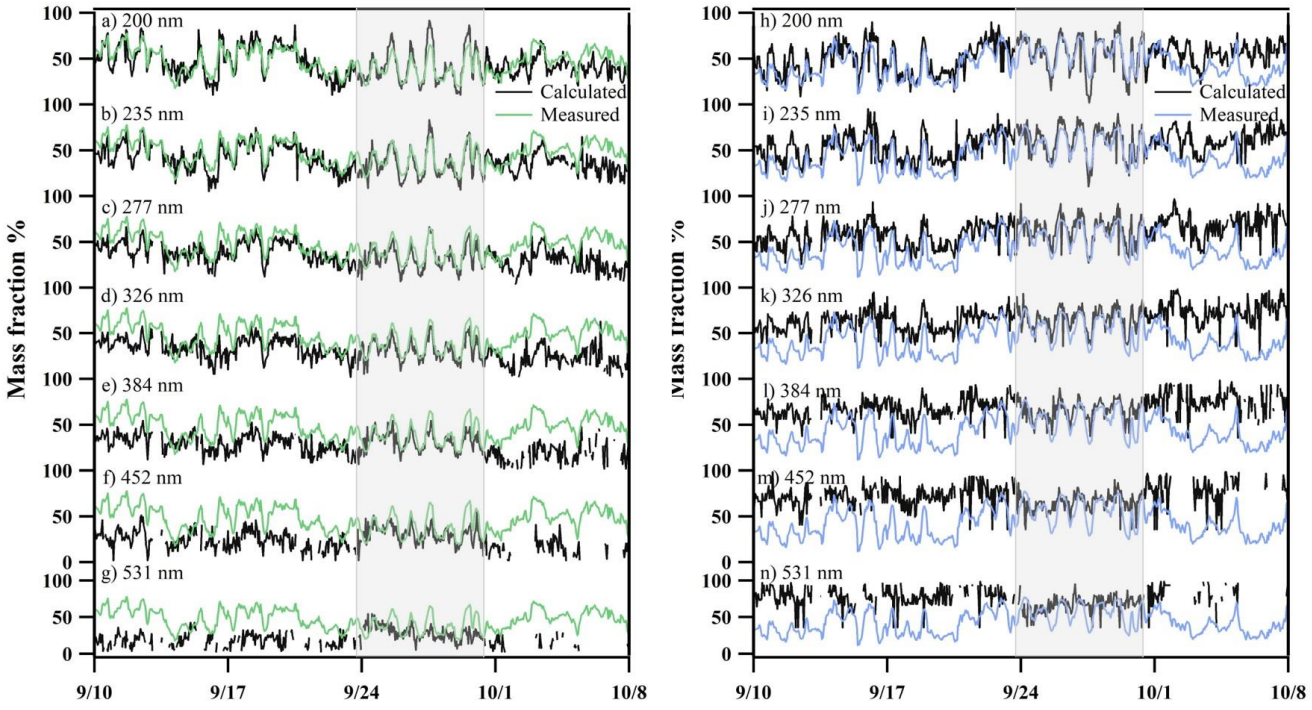

Figure S9: Time series of mass fractions of OAs measured by ACSM and calculated from ρ_{eff} for particles with diameters of (a) 200 nm, (b) 235 nm, (c) 277 nm, (d) 326 nm, (e) 384 nm, (f) 452 nm, and (g) 531 nm. Time series of mass fractions of SIA measured by ACSM and calculated from the ρ_{eff} for particles with diameters of (h) 200 nm, (i) 235 nm, (j) 277 nm, (k) 326 nm, (l) 384 nm, (m) 452 nm, and (n) 531 nm.

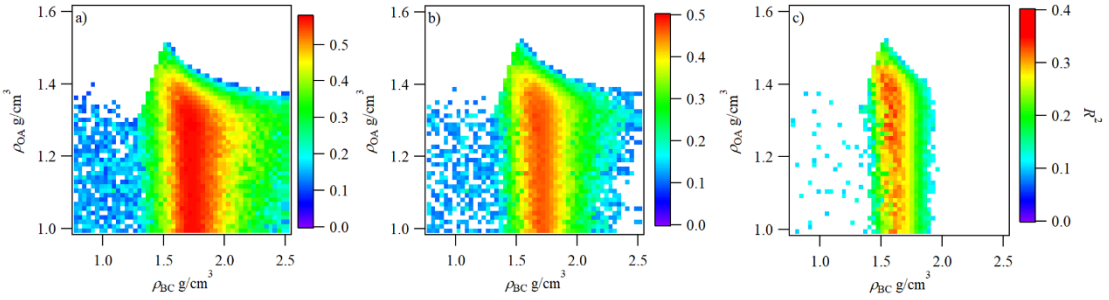

Figure S10: the fitting coefficients of the calculated mass fraction of OAs from the measured ρ_{eff} and the measured mass fraction of OAs with an ACSM for particles with diameters of (a) 200 nm, (b) 235 nm, (c) 277 nm. The OA mass fraction was calculated with ρ_{OA} of 1.0-1.6 g/cm^3 and ρ_{BC} of 0.5-2.5 g/cm^3.

References

Johnson, T. J., Irwin, M., Symonds, J. P. R., Olfert, J. S., and Boies, A. M.: Measuring aerosol size distributions with the aerodynamic aerosol classifier, Aerosol Science and Technology, 52, 655-665, https://doi.org/10.1080/02786826.2018.1440063, 2018.

Tavakoli, F., and Olfert, J. S.: An Instrument for the Classification of Aerosols by Particle Relaxation Time: Theoretical Models of the Aerodynamic Aerosol Classifier, Aerosol Sci. Technol., 47, 916-926, https://doi.org/10.1080/02786826.2013.802761, 2013.

Zhang F., Shen J., Jin J., Shen J., Shi R., Qian H., Song Y., Wei J., Xu Z., Pei X., Wang L., Xu D., Tang Q., Ding J., Wang X., Chen H., Yao L., Tian X., Xu B., and Wang Z.: Unveiling the Chemical Pathways of Secondary Organic Aerosol Formation from mixed biogenic and anthropogenic VOCs in Hangzhou using Explainable Machine Learning, npj Climate Atmos Sci., under review.